Eur. Phys. J. B **47**, 397–409 (2005)
DOI: 10.1140/epjb/e2005-00338-5

THE EUROPEAN PHYSICAL JOURNAL B

Second-order analysis by variograms for curvature measures of two-phase structures

C.H. Arns[1], J. Mecke[2], K. Mecke[3], and D. Stoyan[4,a]

[1] Department of Applied Mathematics, Research School of Physical Sciences and Engineering, Australian National University, Canberra ACT 0200, Australia
[2] Institut für Stochastik, Friedrich-Schiller-Universität Jena, 07740 Jena, Germany
[3] Institut für Theoretische Physik Universität Erlangen-Nürnberg, Staudtstrasse 7, 91058 Erlangen, Germany
[4] Institut für Stochastik, TU Bergakademie Freiberg, 09596 Freiberg, Germany

Received 29 March 2005
Published online 28 October 2005 –

Abstract. Second-order characteristics are important in the description of various geometrical structures occurring in foams, porous media, complex fluids, and phase separation processes. The classical second order characteristics are pair correlation functions, which are well-known in the context of point fields and mass distributions. This paper studies systematically these and further characteristics from a unified standpoint, based on four so-called curvature measures, volume, surface area, integral of mean curvature and Euler characteristic. Their statistical estimation is straightforward only in the case of the volume measure, for which the pair correlation function is traditionally called the two-point correlation function. For the other three measures a statistical method is described which yields smoothed surrogates for pair correlation functions, namely variograms. Variograms lead to an enhanced understanding of the variability of the geometry of two-phase structures and can help in finding suitable models. The use of the statistical method is demonstrated for simulated samples related to Poisson-Voronoi tessellations, for experimental 3D images of Fontainebleau sandstone and for two samples of industrial foams.

PACS. 02.50.-r Probability theory, stochastic processes, and statistics – 05.40.-a Fluctuation phenomena, random processes, noise, and Brownian motion – 81.05.Rm Porous materials; granular materials

1 Introduction

Random geometrical two-phase micro-structures such as porous media, foams, and phase separation processes require an adequate description both for characterization and for calculations of their macroscopic physical properties. It is clear that volume fraction ϕ alone is not sufficient for this purpose. Thus also specific surface s, specific integral of mean curvature and specific Euler number have been considered. These four characteristics are related to the four so-called *'intrinsic volumes'*, which are in 3D space: volume V, surface area S, integral of mean curvature M and Euler characteristic χ.

In a systematic way, these volumes are connected with *'random measures'*. They are defined as follows. Consider a very large random structure X, e.g., the set of all pores of a sample of porous matter, and take the values of the intrinsic volumes for $X \cap B$ for a deterministic test set B. Of course, for different B different values are obtained, which leads to four 'measures' in the sense of the mathematical discipline 'measure theory': measures are functions which assign real numbers to sets and which become 'random measures' for random structures, see [1, Chap. 7] for a short introduction. As usual in many physical studies, we assume here that X is statistically homogeneous and isotropic [2]. Under this condition the mean values of the intrinsic volumes of $X \cap B$ have the form 'constant $\times$ volume of B'. The four constants are just volume fraction ϕ, specific surface s, specific integral of mean curvature and specific Euler characteristic. Because they belong to moments of first order, they are often considered as first order characteristics.

As known in statistics and physics, first order characteristics are valuable descriptors, but often they are not sufficient, as it is well known that quite different structures can have the same first order characteristics. Therefore, it is necessary to refine the description by further characteristics which incorporate variability and spatial correlation. Today, there are three main approaches for variability description of random geometric structures: (i) the use of second-order characteristics, (ii) local porosity distributions [3] and (iii) morphological functions [4–7]. The present paper follows the first and second approach

[a] e-mail: stoyan@orion.hrz.tu-freiberg.de

and demonstrates the use of second-order characteristics, namely pair correlation functions (PCFs) and related characteristics of random measures.

The use of PCFs related to the volume measure and to point fields has a long tradition in Statistical Physics because of its close relation to material properties and scattering experiments. For instance, intensity and angular distribution of light or X-rays passing through a material depend on the fluctuations of dielectric constant and on size and shapes of the regions over which these fluctuations occur, what can be described in kinematic theory by PCFs. Since the very first X-ray scattering experiments [8], PCF became almost a synonym for structural analysis in physics. Not only can physical properties such as dielectric constant be obtained from scattering data but also the size and shape of inhomogeneities; within the Born approximation the scattered intensity of X-rays is proportional to the Fourier transform of the PCF of the scatterer. Because of the importance of structural analysis in condensed matter physics, analytical expressions of regular bodies [9] as well as large/small wave-vector approximations [10–13] and PCFs of stochastic models [14–16] were derived.

Previously, this approach has been generalized to consider (i) PCFs related also to intrinsic volumes different to usual volume and (ii) characteristics of orders higher than two. The most general exposition of this kind is probably given in reference [17]. Because of the unsystematic evolution of the statistical theory, the notation for second-order characteristics and intrinsic volumes has to date been unsystematic. The present paper suggests a unified notation, assigning to the characteristics indices equal to the dimensions of the corresponding intrinsic volumes. Normalized densities are denoted by g, while corresponding integrated characteristics are denoted by k. Here traditions of point process statistics and random set statistics are used. Finally, variograms are denoted by γ, following the traditions of geostatistics.

Second-order characteristics play three different roles: (1) They serve in a statistical sense as *descriptors* of variability and spatial correlation, which give, for example, information about the range of correlation in the structure or help to find suitable statistical models for simulations. (2) PCFs and intrinsic volumes are used in physical calculations of *macroscopic properties* starting from microstructure information [18,19]. (3) Finally second-order characteristics serve in *reconstruction* simulations [20,21] as reference functions, often combined with morphological functions. Clearly, second-order characteristics are one (very important) possibility to characterize spatial structures, but there are other methods, for example higher-order characteristics or morphological functions. And they represent some form of data compression which averages out a lot of distributional information.

In the present paper the first case is considered, and the data are voxelized, which result from simulation and experimental tomographic images. We show how the second-order characteristics can be determined statistically, in particular, for the cases of surface area S and Euler characteristic χ. This is a difficult task because the best characteristics, the PCFs g, have the character of density functions, while voxel data are discrete. Therefore this paper considers characteristics of an integrated or smoothed nature, namely total values measured over spheres. An example is the total surface area $S(x;R)$ of the structure X in the test sphere $b(x,R)$ of radius R centered at point x – analysed as a function of x. For radii R not too small, methods of discrete geometry can be used to obtain precise values of these quantities, even for the cases of the curvature characteristics M and χ. While the local porosity approach [3] considers the one-dimensional distributions of these values, we study here the spatial behaviour of such values for spheres with different centres x. This leads to *random fields of intrinsic volumes*, i.e., families of random variables indexed by points x in space. They can be statistically analysed by methods of geostatistics, see [22]. The close relationship between the corresponding second order characteristics of the field, called *'variogram'*, and the pair correlation function of the random measures can be used for their statistical estimation.

The paper is organised as follows: Section 2 introduces intrinsic volumes and curvature measures. While these quantities are defined and investigated in the mathematical literature for very general geometrical structures, here they are explained in Sections 2 and 3 only for 'smooth' structures. Section 3 introduces various statistical functions including PCFs but also variograms, which are useful for the description of second-order properties of all four intrinsic volumes. In order to support the understanding and interpretation of empirical results, Section 4 discusses two very simple stochastic models, which are reminiscent of closed-cell and open-cell foams. While they do not satisfy the smoothness assumptions of Section 2, their structure is clear and calculation of their pair correlation functions is easy. Section 5 then describes statistical methods, in particular those based on variograms related to random fields of sphere contents. This can be considered as a spatial extension of the local porosity approach [3]. The final Section 6 demonstrates the application of the statistical methods to various data sets, including simulated models and real experimentally imaged samples.

2 Intrinsic volumes and curvature measures

For a body Y in R^3 with sufficiently smooth surface there are four natural geometrical characteristics of different dimensionality, namely volume $V(Y)$, surface area $S(Y)$, integral of mean curvature $M(Y)$, and integral of total curvature $K(Y)$;

$$\begin{aligned} S(Y) &= \int_{\partial Y} ds\,, \\ M(Y) &= \int_{\partial Y} \frac{1}{2}\Big(\frac{1}{r_1(s)} + \frac{1}{r_1(s)}\Big)\, ds\,, \\ K(Y) &= \int_{\partial Y} \frac{1}{r_1(s)\; r_2(s)}\, ds\,, \end{aligned} \tag{1}$$

where ∂Y is the surface of Y and $r_1(s)$ and $r_2(s)$ are the maximum and minimum curvature radii in s. $M(Y)$ is also called the integral of Germain's curvature and $K(Y)$ integral of Gaussian curvature; $\chi(Y) = K(Y)/4\pi$ is called Euler characteristic. In the mathematical literature more general definitions are given, which are valid also in cases of reduced smoothness properties [23,24].

Integral geometry [23,24] shows that these characteristics and their counterparts in d-dimensional space play a fundamental role. A famous example is Hadwiger's theorem, saying that additive, motion-invariant, and continuous functionals of convex sets are linear combinations of these four characteristics. Up to constant factors these characteristics are proportional to the *Minkowski functionals* $W_i(Y)$:

$$\begin{aligned} W_0(Y) &= V(Y), \\ W_1(Y) &= \frac{1}{3}S(Y), \\ W_2(Y) &= \frac{1}{3}M(Y), \\ W_3(Y) &= \frac{1}{3}K(Y) = \frac{4\pi}{3}\chi(Y). \end{aligned} \tag{2}$$

Since the numbering of Minkowski functionals is a bit unnatural, modern integral geometers use the *intrinsic volumes* $V_k(Y)$ [24] which in R^3 are;

$$\begin{aligned} V_0(Y) &= \chi(Y), \\ V_1(Y) &= \frac{1}{\pi}M(Y), \\ V_2(Y) &= \frac{1}{2}S(Y), \\ V_3(Y) &= V(Y). \end{aligned} \tag{3}$$

Starting from intrinsic volumes, one can define *curvature measures*. For a given (and then fixed) random structure X the random curvature measures $C_{X,i}$ are defined for a variable set B in $\mathbb{R}^3$ as follows:

$$C_{X,i}(B) = V_i(X \cap B). \tag{4}$$

Particular cases are the *volume measure* $V_X(B)$, *surface measure* $S_X(B)$, and *total curvature measure* $K_X(B)$:

$$\begin{aligned} V_X(B) &= V(X \cap B) = C_{X,3}(B), \\ S_X(B) &= S(\partial X \cap B) = 2C_{X,2}(B), \\ K_X(B) &= \int\limits_{\partial X \cap B} \frac{1}{r_1(s)\ r_2(s)}\ ds = 4\pi C_{X,0}(B). \end{aligned} \tag{5}$$

For $i = 0, 1$ and 2 the measures are completely concentrated on the surface ∂X of X. For $i = 0$ and 1 the curvature measures can have negative values, i. e. these measures are 'signed' measures. For definitions of curvature measures for more general structures see [23,24]. Note that in the local porosity approach only the distribution of quantities related to $V_X(B)$ is considered.

3 Intensities and pair correlation functions

The means of the random curvature measures are (non-random) measures, which have a very simple form in the case of statistical homogeneity:

$$\langle C_{X,i}(B) \rangle = c_i V(B), \quad \text{for} \quad i = 0, ..., 3, \tag{6}$$

where $V(B)$ is the usual volume of B. The c_i depend of course on X, but this dependence is depressed in the notation. The c_i are called *curvature intensities* and are known by more traditional names and symbols: c_3 is the volume fraction, frequently used symbols are ϕ and V_V; $c_2 = \frac{1}{2}s$ is the half specific surface s, frequently used symbols for the latter are s and S_V; c_1 is denoted by M_V, and c_0 is often called specific connectivity number, specific Euler number or density of Euler number and denoted by N_V or χ_V.

The second order behaviour of homogeneous and isotropic random measures is described by product densities, pair correlation functions and so-called K functions. The aim is to express means such as

$$\langle C_{X,i}(A)\, C_{X,j}(B) \rangle \tag{7}$$

for two test sets A and B. A particular case is the *variance* $\sigma_i^2 = var(C_{X,i}(B))$ of $C_{X,i}(B)$ for a given set B. The following formulas for such quantities are given for smooth structures (see Ref. [1], Sect. 7.2). The first one is

$$var(C_{X,i}(B)) = c_i^2 \int\limits_0^\infty \overline{\gamma}_B(r) dK_i(r) - (c_i V(B))^2, \tag{8}$$

where $\overline{\gamma}_B(r)$ is the isotropized set covariance of B [1, p. 233], and K_i the K *function* of $C_{X,i}$. The differential $dK_i(r)$ can be replaced via

$$c_i^2 dK_i(r) = 4\pi r^2 \rho_i(r)\ dr \tag{9}$$

and

$$dK_i(r) = 4\pi r^2 g_i(r)\ dr. \tag{10}$$

Here $\rho_i(r)$ denotes the *product density* and $g_i(r)$ the *pair correlation function of* $C_{X,i}$. All $g_i(r)$ for $i \leq 2$ satisfy $g_i(0) = \infty$ and $g_i(\infty) = 1$. The interpretation of $\rho_i(r)$ and $K_i(r)$ is as follows: consider two infinitesimally small balls b and b' of volumes dV and dV' at distance r. Take the mean $m_i(r)$ of the product of $C_{X,i}(b)$ and $C_{X,i}(b')$. Then

$$m_i(r) = \rho_i(r) dV dV'. \tag{11}$$

Further consider a point randomly chosen in X ($i = 3$) or in ∂X ($i = 0, 1, 2$) and take it as centre of a ball $b(r)$ of radius r. Then $c_i K_i(r)$ is the mean of $C_{X,i}(b(r))$. Consequently the variance formula (8) can be rewritten as

$$\text{var}(C_{X,i}(B)) = c_i^2 \int\limits_0^\infty 4\pi\ r^2\ \overline{\gamma}_B(r)\ [g_i(r) - 1]\ dr, \tag{12}$$

using the formula

$$4\pi \int\limits_0^\infty \overline{\gamma}_B(r) r^2 dr = (V(B))^2\,, \tag{13}$$

which is valid for arbitrary B. For a sphere of radius R it is

$$\overline{\gamma}_B(r) = \frac{4}{3}\pi R^3 \left(1 - \frac{3r}{4R} + \frac{r^3}{16R^3}\right) \tag{14}$$

for $r < 2R$, otherwise it vanishes. It can happen that $g_i(r) = 1$ for all $r \geq r_0$ for some r_0. Then this r_0 is called *range of correlation*. If r_0 is infinite, then the range of correlation is that value r_0 for which $|g_i(r) - 1| < \epsilon$ for all $r \geq r_0$. The term 'range of correlation' is also used in a qualitative sense by saying that the range of correlation for one structure and characteristic is larger than for another if the speed of the convergence of $g_i(r)$ towards 1 is faster.

Some of these second order characteristics are well-known in the physics literature and used in many applications. Clearly, $\rho_3(r)$ is the same as the covariance $C(r)$ (as in [1] and other references) or the two-point probability function $S_2(r)$ as in [2]. Finally, second order characteristics related to $i = 0$ appear in [25]. The form of $S_2(r)$ is known for various models, see [1,2,26]. It is $S_2(0) = \phi$ and $S_2(\infty) = \phi^2$. For Boolean models [1,27], $S_2(r)$ is monotonously decreasing, while for sphere packings it shows additional oscillations [2,26].

Furthermore, formulas for $\rho_2(r)$, which coincides with the surface correlation function $F_{ss}(r)$, are given in [2, Eq. (6.18) and p. 170], for Boolean models with spherical grains. A Boolean model is a random set formed by the set-theoretic union of fully penetrable grains; see [1] for a precise definition. The corresponding $F_{ss}(r)$ has a pole at $r = 0$, is monotonously decreasing and is equal to $s^2 = S_V^2$ for r larger than the largest sphere diameter; if the diameters are constant equal to R, then at $r = 2R$ there is a small discontinuity. For Boolean models with spherical grains, formulae are derived in references [4,17,28] and are numerically tested in reference [29] for the product densities of all intrinsic volumes, including that for the Euler characteristic. Figure 1 shows, for instance, the pair correlation function $g_0(r)$ for the planar Boolean model with circular grains of radius R and intensity $n = \pi R^2 \lambda$, where λ is the density of the underlying Poisson point process. In contrast to $g_2(r)$ or $g_3(r)$ one finds not only a discontinuity at $r = 2R$ but a singularity of $g_0(r)$ because the Euler characteristic $V_0(P)$ does not vanish for a single point P where two discs intersect at contact.

In addition to variances 'mixed' moments can also be considered, namely quantities such as $\langle C_{X,i}(A)\, C_{X,j}(B)\rangle$ for two different sets A and B. An important special case, in particular where $i = j$, is $A = B_{\mathbf{r}} = \{y : y = z + \mathbf{r}, z \in B\}$ for any vector $\mathbf{r} = r\mathbf{e}$, where A is a shifted copy of B. Similar to equation (8) the mixed moment corresponding to these sets A and B, called the covariance function, can be expressed in a formula. For the spherical case of $B = b(o, R)$ it is

$$\begin{aligned} k_i(r) &= \langle C_{X,i}(B) C_{X,i}(B_{\mathbf{r}})\rangle \qquad (15)\\ &= 2\pi c_i^2 \int_{r'=0}^{2R} \overline{\gamma}_B(r')\, r'^2 \int_0^{\pi} \sin\beta\; g_i(s(r',\beta))\; d\beta dr', \end{aligned}$$

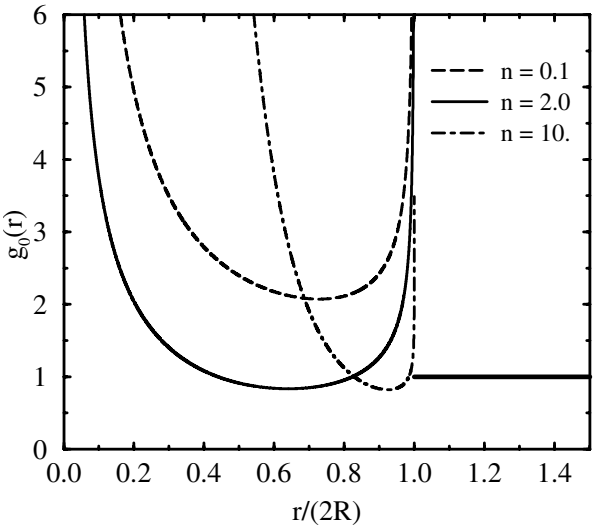

Fig. 1. Pair correlation function $g_0(r)$ for the planar Boolean model with circular grains of radius R and intensity $n = \pi R^2 \lambda$. Note the non-monotonuous behaviour of $g_0(r)$ in the intensity n which is already visible in the curvature intensity $c_0(n)$ as function of n.

where $s(r', \beta) = \sqrt{r'^2 + r^2 - 2rr'\cos\beta}$. For small R such that $\rho_i(x) \approx \rho_i(r)$ for $r - 2R \leq x \leq r + 2R$, equation (13) leads to

$$k_i(r) \approx \rho_i(r)(V(B))^2. \tag{16}$$

In this approximation discontinuities and poles of $\rho_i(r)$ (and $g_i(r)$) are smoothed away. Nevertheless, equation (16) yields useful estimates of $\rho_i(r)$, if B and equivalently R are small.

Finally, moments of the type given in equation (7) can be considered for $i \neq j$. This leads to mixed product densities $\rho_{ij}(r)$ etc. In [2] the example $i = 3$ and $j = 2$ is considered; instead of $\rho_{32}(r)$ the symbol $F_{sv}(r)$ is used. In references [4,17] formulae are derived for such functions for Boolean models with an application to galaxy distributions given in [28].

4 Pair correlation functions for foam models

We consider two random model structures, which serve as simple stochastic models for foams. Their volume fraction ϕ is zero and they are not smooth in the sense of Section 2. But they are easy to understand and the calculation of their second-order characteristics is simple. These two examples serve to show that there are random structures X where the pair correlation functions $g_i(r)$ can qualitatively differ for different dimensions i.

The basis of both models is the Poisson plane process [1], an infinite system of random planes in R^3. The mean surface area per volume unit of this plane system is denoted by s. These planes generate a random network X of lines of intersection. This network is the first random structure studied here, called *Poisson network* in the following; it could be considered as a simple model for

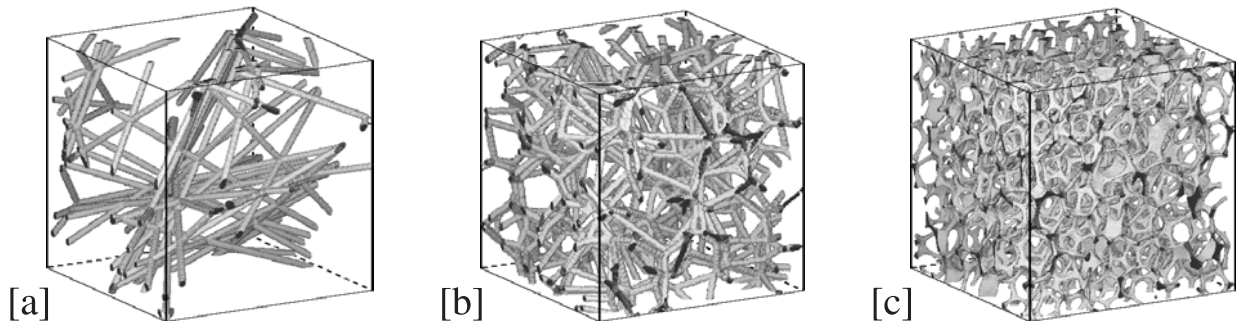

Fig. 2. Network-like structures. [a] Lines of intersection of a Poisson plane process or Poisson network, [b] Voronoi network, [c] Aluminium foam of size $(17.3\,\mathrm{mm})^3$ at $32\,\mu$m resolution [30].

an open-cell foam. This model could be a starting point for the construction of physically more realistic models by extending the lines to infinite cylinders as shown in Figure 2a.

One could construct a similar model starting from the edges of a Voronoi tessellation as in Figure 2b, but this model is analytically intractable. However, numerical results are studied together with a real open-cell foam (Fig. 2c) in Section 6.

The Poisson network X can be described by the length measure L_X, where $L_X(B)$ = total length of all line pieces in the set B. The corresponding pair correlation function $g_1^L(r)$ can be easily obtained by the methods described in Chapter 9 of [1]. It is

$$g_1^L(r) = 1 + \frac{2}{sr} + \frac{4}{\pi^2 s^2 r^2}. \tag{17}$$

We assume that qualitatively the behaviour of $g_1^L(r)$ is similar to that of the pair correlation functions $g_2(r)$ and $g_3(r)$ of the Poisson network mentioned above. Because the network consists only of lines, its curvature measure $C_{X,0}$ is completely concentrated in those points in which three planes intersect. Each of these points contributes –2 to $C_{X,0}$. Thus $g_0(r)$ equals the pair correlation function $g_0^P(r)$ of the point process of plane intersection points, which is

$$g_0^P(r) = 1 + \frac{9}{2sr} + \frac{36}{\pi^2 s^2 r^2}. \tag{18}$$

The corresponding intensity is $c_0 = -\pi s^3/24$. Figure 3 shows both pair correlation functions $g_1^L(r)$ and $g_0^P(r)$ for $s = 1$, which display a similar behaviour.

The second random structure, called *Poisson plane model*, has a different geometry. Let now X be the system of all planes of the Poisson plane process and let on all planes independent identically distributed planar point fields be scattered. Their points mark holes of diameter 0 in the planes. This structure would be physically more realistic if the planes are replaced by infinite plates of positive thickness with holes of positive diameter. Without such holes we would speak about a closed-cell foam. Figure 4 shows three structures, a Poisson plane process, a closed-cell Voronoi structure, as well as a real foam which

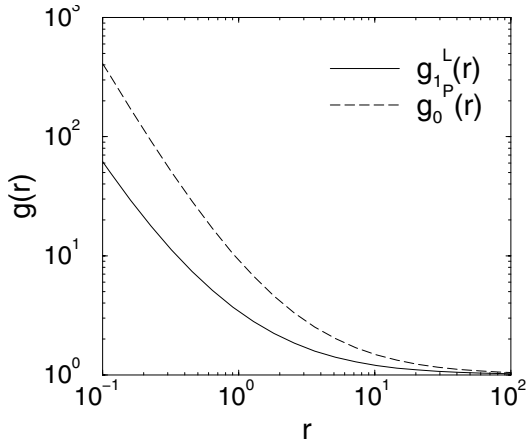

Fig. 3. Pair correlation functions $g_1^L(r)$ and $g_0^P(r)$ of the network model for $s = 1$ (see Eqs. (17, 18)).

is almost closed-cell, with holes between some cells. The second order characteristics of the last two models are considered in Section 6.

This plane system X with holes can be described by the surface measure S_X, where $S_X(B)$ = total area of all plane pieces in the set B. Since the holes are points, they do not contribute to S_X. The corresponding K function is given in [1, p. 302], which yields the pair correlation function $g_2^S(r)$ as

$$g_2^S(r) = 1 + \frac{1}{2sr}. \tag{19}$$

For planes the curvature measure $C_{X,0}$ is concentrated in the plane intersection points and in the holes; they contribute 1 and -1, respectively, to $C_{X,0}$. Defining the density (=mean number of points per area unit) of the point fields of holes by λ_h and its pair correlation function by $g_h(r)$, one obtains;

$$g_0^P(r) = 1 + \left(\frac{\pi^2 s^5}{512} - \frac{\pi\lambda_h s^3}{16} + \frac{s\lambda_h^2 g_h(r)}{2}\right)\frac{1}{cr} + \frac{s^4}{64}\,\frac{1}{cr^2} \quad \text{with} \quad c = s^2\left(\frac{\pi s^2}{48} - \lambda_h\right)^2. \tag{20}$$

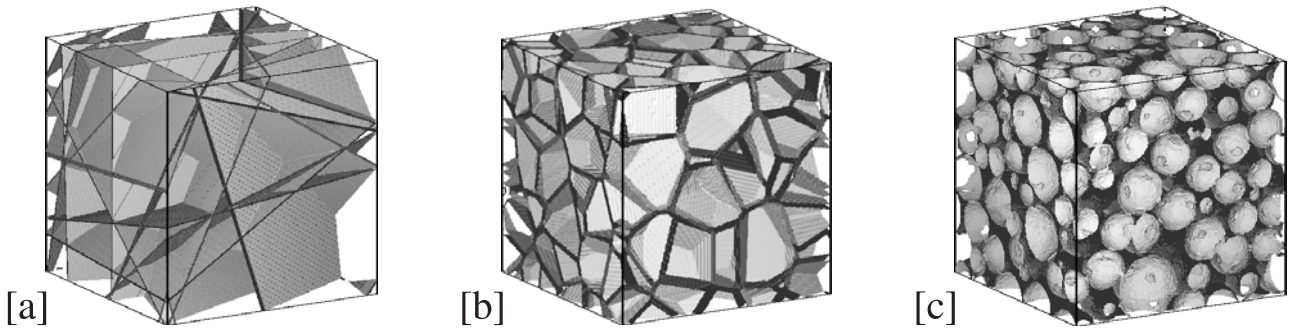

Fig. 4. Closed cell structures. [a] Poisson plane process, [b] Voronoi cell model, [c] industrial foam with some holes between cells (subsection of size $(1.68\,\mathrm{mm})^3$, sample A of [31]).

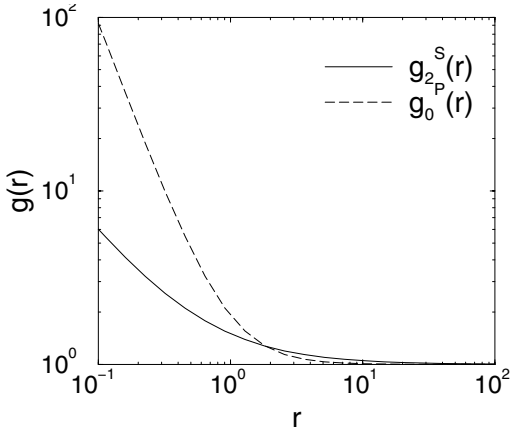

Fig. 5. Pair correlation functions $g_2^S(r)$ and $g_0^P(r)$ of the plane model (see Eqs. (19, 20)), for $s = 1$, $\lambda_h = \frac{\pi}{16}$ and a Poisson process of holes.

The corresponding intensity is $c_0 = \pi s^3/48 - s\lambda_h$. For $\lambda_h = 0$ the case of closed-cell foam is obtained where equation (20) reduces to equation (18). Figure 5 presents the functions $g_2^S(r)$ and $g_0^P(r)$, where the parameters are $s = 1$ and $\lambda_h = \frac{\pi}{16}$ and the pair correlation function is $g_h(r) = 1$, corresponding to a Poisson process. Both curves have a parabolic form, but $g_0^P(r)$ approaches the value 1 much faster than $g_2^S(r)$. So one may say that the range of correlation of the two-dimensional surface measure is larger than that of the zero-dimensional Euler measure. This can be explained by the negative values of the Euler measure at the holes, which compensate for positive values at intersection points and thus reduce the variability.

5 Statistical methods: numerical estimation of pair correlation functions

5.1 Volume measure

In the case of the volume measure V_X, the product density $\rho_3(r)$ is the classical two-point probability function $S_2(r)$. The statistical methods for the estimation of $S_2(r)$ are well known. Naïve estimation methods simply follow the definition. For the case of small samples, more sophisticated methods were developed, where edge correction plays an important role, see [32]. For large samples in 3D space, Fourier methods as described in [33,34] are useful. This method was used here to calculate the variograms of the experimental datasets. The two-point probability function $\rho_3(r)$ was calculated by a straight convolution of the volume characteristic function in Fourier space using padding to prevent wrap-around errors (i.e. [35]).

5.2 Surface measure

The estimation of the product density $\rho_2(r)$ of the surface measure S_X is more complicated than that of $\rho_3(r)$. The difficulty results from the fact that $\rho_2(r)$ has the character of a density function which is related to a random surface. If the data are given as voxel data (as assumed in the present paper) then the surface is given only in some approximation and the determination of $\rho_2(r)$ for small r is difficult. For small r, the product density $\rho_2(r)$ has a delicate behaviour since it has a pole of order -1 at $r = 0$.

The methods described in [36] and [2, p. 285], are useful for simulated data which include all details in Euclidean space, but not for voxelized data. There are several methods which yield approximations of $\rho_2(r)$ for voxelized data. One is the geostatistical method described in a general context in the following section.

5.3 Variograms of curvature measures

A fruitful statistical idea consists in assigning a random field to a random measure and then to analyse the random field. In the given case, for $i = 0, 1, 2$ and 3 the random field $Z_i(x)$ is defined as in the local porosity approach by

$$Z_i(x) = C_i(b(x, R)) \qquad \text{for} \qquad x \in \mathbb{R}^3. \tag{21}$$

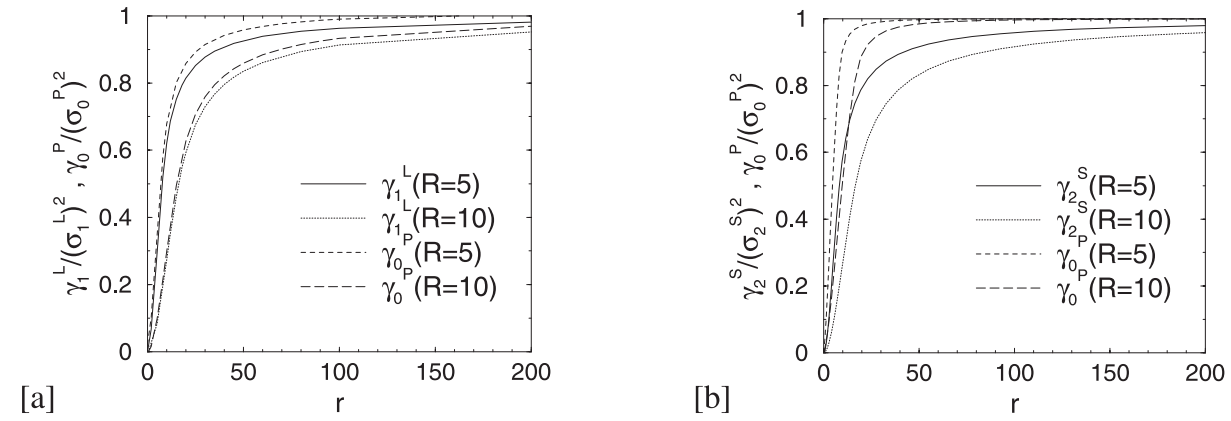

Fig. 6. Normalized variograms for radii $R = 5$ and $R = 10$ of [a] the network model (see Fig. 2a) for length (L) and Euler number (P) (corresponding pair correlation function shown in Fig. 3) and [b] the plane model (see Fig. 4a) for surface (S) and Euler number (P) (corresponding pair correlation function shown in Fig. 5).

Here the sphere radius R is considered as a parameter, which has of course influence on the behaviour of the random field. Mean m_i, variance σ_i^2 and one-dimensional distribution of the random field are location independent because of the homogeneity assumption. One finds

$$m_i = c_i \cdot \frac{4}{3}\pi R^3, \tag{22}$$

while σ_i^2 is given by equation (8). Of course, one can use other observation windows than a sphere $b(x, R)$. While Hilfer [3] and Torquato [2] consider only the one-dimensional distribution of the random field, we study here also its spatial correlations. Appropriate methods have been developed in geostatistics (see e.g. [22]).

The usual geostatistical characteristic in such analyses is the variogram $\gamma(r)$, here for $Z_i(x)$ denoted by $\gamma_i(r)$,

$$\gamma_i(r) = \frac{1}{2}\langle (Z_i(o) - Z_i(\mathbf{r}))^2 \rangle, \tag{23}$$

where $\mathbf{r}$ is any point in R^3 of distance r from o. The variogram can also be expressed in terms of the covariance function (see Eq. (15)) as

$$\gamma_i(r) = \sigma_i^2 - k_i(r) + m_i^2. \tag{24}$$

Thus statistical analyses which yield variograms $\gamma_i(r)$ also lead to $k_i(r)$ and by applying the approximation (16) to smoothed versions of $\rho_i(r)$ and $g_i(r)$. The range of correlation can be found also by means of the variogram. Here the convergence towards σ_i^2 is the criterion.

Of course, the parameter R plays an important role. For a small radius R one can expect that equation (16) works well. However if R is large, $k_i(r)$ gives only little information about the structure X and is mainly determined by the set covariance $\overline{\gamma}_B(r)$ (see Eq. (8)). For $B = b(o, R)$ and large R, $\gamma_i(r)$ takes the form of the so-called spherical variogram (see Eq. (14)), where

$$\gamma_i(r) \propto \frac{3}{2}\,\frac{r}{2R} - \frac{1}{2}\Big(\frac{r}{2R}\Big)^3. \tag{25}$$

Applying equations (15) and (24) one may transform pair correlation functions $g_i(r)$ into variograms $\gamma_i(r)$. Figure 6 shows variograms for the Poisson network and plane model for two radii R. Clear differences in the ranges of correlation for different characteristics of the same geometrical structures are visible. Note, that $\gamma_i(r \to \infty) \to \sigma_i^2$ (see Eq. (8)).

6 Applications on foams and porous media

6.1 Poisson-Voronoi foams

To illustrate further the method introduced in the previous section two foams are considered here which are related to the 3D Voronoi tessellation of point distribution of a Poisson point process. One of the foams is an open-cell foam and obtained from the cell edges of the tessellation by enlarging them to cylinders of diameter d. Figure 2b shows a simulated sample with intensity of the underlying Poisson process $\tau = 100\,\mathrm{mm}^{-3}$ and $d = 12.5\,\mu$m. The other is a closed-cell foam and obtained by enlarging the cell faces to plates of thickness t. Figure 4b shows a simulated sample with the same τ and $t = 5\,\mu$m. The mean cell volume of the underlying tessellation is $0.01\mathrm{mm}^3$ and the mean side length is $93\,\mu$m. We simulated both models in a cube of side length 1 mm and then determined the variograms numerically by approximating the cell structure by a voxel set. The results are shown in Figures 7 and 8.

For the network model or open-cell foam the variograms for volume and surface coincide and show a range of correlation of approx. 0.15 mm, while the range of correlation for the Euler characteristic is much shorter, about 0.05 mm. For all four intrinsic volumes the variograms do not show pronounced oscillations, indicating the high degree of irregularity which is inherited from the Poisson process of cell centres to the system of edges of the tessellation.

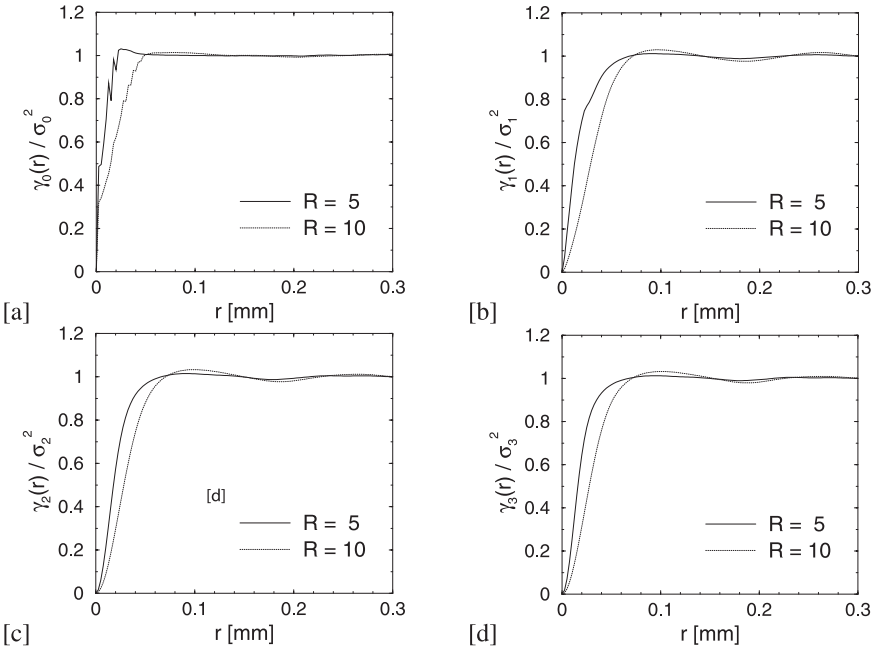

Fig. 7. Normalized variograms $\gamma_i(r)$ of the intrinsic volumes and curvature measures $C_{X,i}(B)$ of the Voronoi network model (Fig. 2b) for $R = 5$ and $R = 10$ voxels. [a] Euler characteristic, [b] integral mean curvature, [c] surface area, [d] volume.

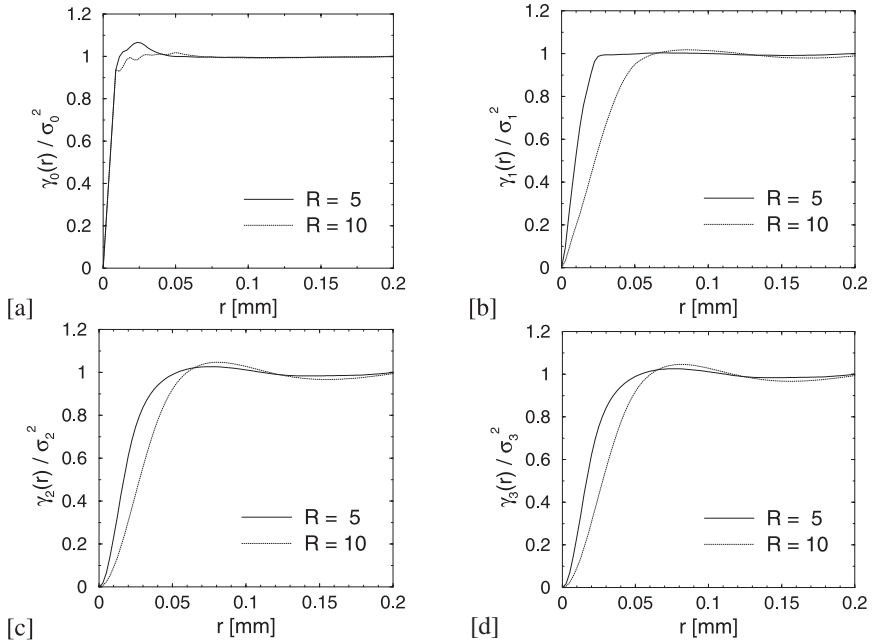

Fig. 8. Normalized variograms $\gamma_i(r)$ of the intrinsic volumes and curvature measures $C_{X,i}(B)$ of the Voronoi cell model (Fig. 4b) for $R = 5$ and $R = 10$ voxels. [a] Euler characteristic, [b] integral mean curvature, [c] surface area, [d] volume.

For the Voronoi cell model or closed-cell foam again the variograms for volume and surface are similar, but now they indicate some local regularity as there are oscillations with a maximum at 0.05 mm and a minimum at 0.15 mm. The range of correlation is here about 0.2 mm, a bit longer than for the network model. The stronger spatial correlation shows that the irregularity of the Poisson-Voronoi tessellation is different if faces and if edges are considered. Again the variogram for the Euler characteristic is quite different, indicating only slight spatial correlation (and a high degree of variability); the range of correlation seems to be less than 0.05 mm.

6.2 Industrial foams

Let us now consider physical foam samples. Both industrial foam images analysed in this section were acquired on the ANU micro-CT facility. The open-cell foam of Figure 2c shows the full size (540^3 voxel or $17.3\,\mathrm{mm}^3$) of a subset of a 1024^3 image acquired at $32\,\mu$m resolution (see also [30]). The closed-cell foam of Figure 4c represents a

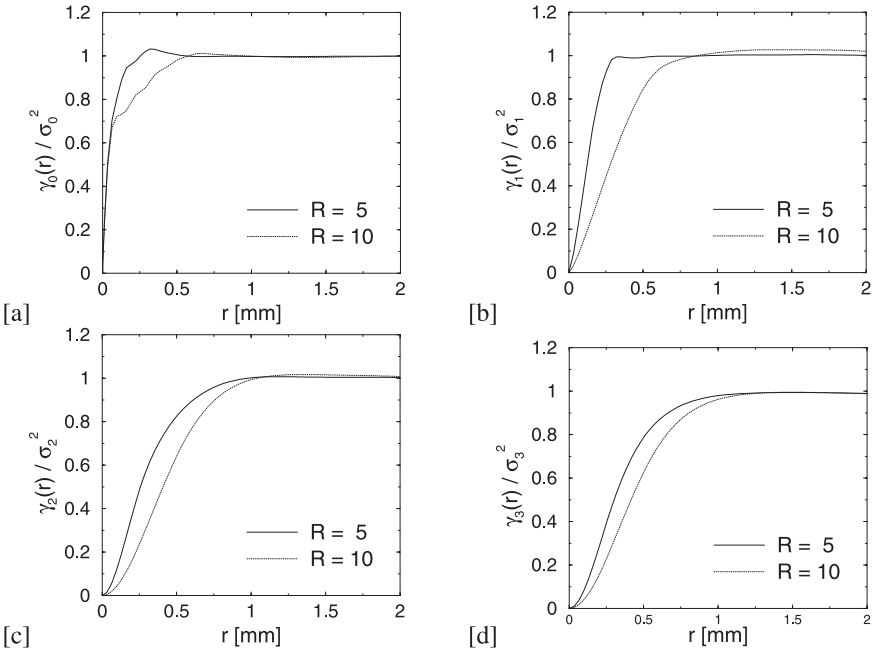

Fig. 9. Variograms $\gamma_i(r)$ of the intrinsic volumes (curvature measures) $C_{X,i}(B)$ of the Aluminium foam (Fig. 2c) for $R = 5$ and $R + 10$ voxels. [a] Euler characteristic χ_V, [b] integral mean curvature M_V, [c] surface area S_V, [d] volume V_V.

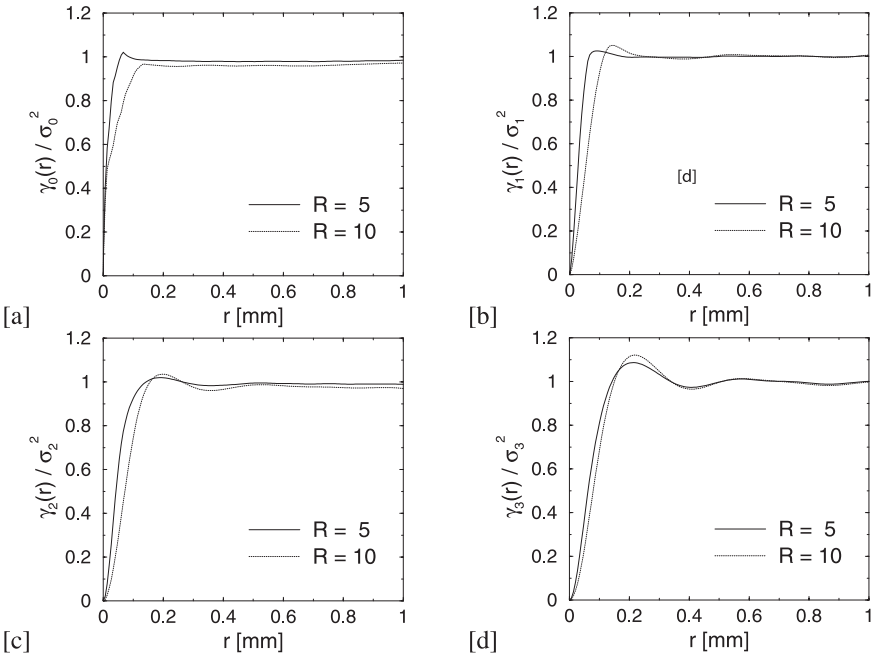

Fig. 10. Variograms $\gamma_i(r)$ of the intrinsic volumes (curvature measures) $C_{X,i}(B)$ of the industrial foam (Fig. 4c) for $R = 5$ and $R = 10$ voxels. [a] Euler characteristic χ_V, [b] integral mean curvature M_V, [c] surface area S_V, [d] volume V_V.

subset of the $456 \times 456 \times 912$ (about $58\,\mathrm{mm}^3$) central section of a 1024^3 image at $6.7\,\mu$m resolution analysed here, and has previously been studied in [31,37].

For details of the reconstruction and segmentation process see [30,38]. This study analyses the resulting binary phase images. Figures 9 and 10 show the variograms obtained for the open- and closed-cell foams respectively.

For the *open-cell foam* of Figure 2c the variograms for volume and surface nearly coincide, they show a range of correlation of 1 mm. In contrast, the ranges of correlation for the integral of mean curvature and for the Euler characteristic are clearly shorter, about 0.25 mm. All four variograms indicate only little regularity, as they all do not have any oscillations with pronounced maxima and minima.

This is different to the *closed-cell foam* of Figure 4c. There for volume and surface area oscillations are clearly visible, indicating local regularity in size and arrangement

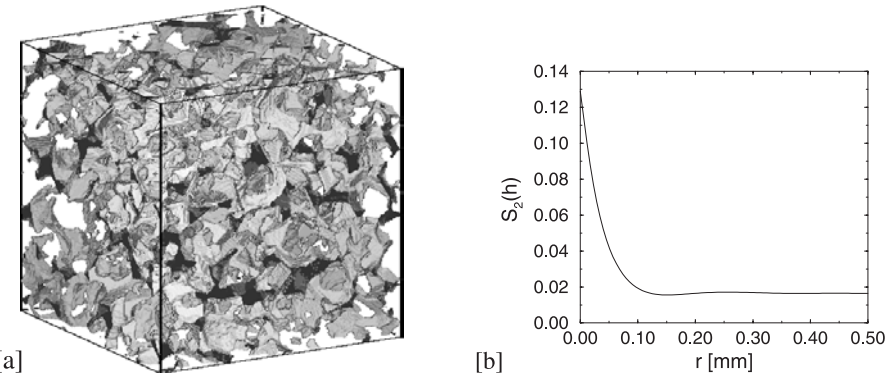

Fig. 11. Fontainebleau sandstone. [a] Pore-grain interface of a $(1.4\,\mathrm{mm})^3$ subsection of a Fontainebleau sandstone with 13% porosity. [b] Two-point volume to volume correlation function of the pore space.

of the cells, which is obviously more pronounced than for the sandstone discussed in the following section. In contrast, the integral of mean curvature and the Euler characteristic are more irregularly distributed. These differences are also clearly expressed by the different ranges of correlation, which are 0.05 mm for Euler and 0.6 mm for volume.

6.3 Fontainebleau sandstone

The homogeneity of Fontainebleau sandstone in composition, grain size, and porosity makes it an ideal system for comparative studies. Other statistical-morphological studies of such material were published in [3,20,21,39–42]. In [39] permeability was calculated on five sub-volumes of different sizes (between 0.085 mm^3 and 0.59 mm^3) at a resolution of 10 μm and a relatively large variability resulted. In [40] reasonable averaging of permeabilities was found for eight sub-volumes of 0.59 mm^3 at a resolution of 7.5 μm. In [42] a 33.6 mm^3 volume of Fontainebleau sandstone at 6.3 μm resolution was analysed by sub-sampling and evaluating local porosity, percolation, and conductivity distributions to test a reconstruction technique based on inscribed spheres. It was found that porosity does correlate poorly to conductivity.

We consider a sample of Fontainebleau sandstone, which was already analysed in [43–47]. These previous studies found the scatter in permeability over porosity to be larger than for effective elastic moduli, effective conductivity, or the morphological measures. This suggests that representative volumes (if they exist) exhibit different sizes for different physical properties, a notion important in up-scaling. The reconstructed image has a resolution of 5.68 μm and was thresholded using a kriging-based thresholding method [48] to give a binary solid-pore image [49,43]. A 480^3 cubic subset was extracted for analysis, corresponding to a volume of $20.5\,\mathrm{mm}^3$. A picture of a 240^3 subsection of this sample is given in Figure 11a. Figure 11b shows the empirical two-point probability function $S_2(r)$ for the sample. The solid volume fraction of the sample is $V_V = 0.871$, specific surface $S_V = 15.5\,\mathrm{mm}^{-1}$, specific mean curvature $M_V = -235\ \mathrm{mm}^{-2}$, and specific Euler characteristic $\chi_V = -175\ \mathrm{mm}^{-3}$. For S_V, the digital analysis gives $S_V = 15.5\,\mathrm{mm}^{-1}$. However, the grains are not aligned with the lattice directions and it is generally recognised that the surface area of a sphere in the continuum is a a factor of 2/3 smaller (e.g. [50]). Thus the real value is closer to $S_V = 10.3\,\mathrm{mm}^{-1}$. The negative value of χ_V is typical for bicontinuous porous media with few isolated components. Visual inspection by comparing Figures 4b and 11a shows that perhaps a plane model is more similar to the sandstone structure than an open-cell foam.

6.3.1 Structural analysis

It was calculated from the whole data set of 480^3 voxels by convolution in Fourier space. As it has to be, for $r = 0$ the value V_V appears and for large r the value $V_V^2 = 0.0166$. There is a local minimum at $r = 0.15$ mm and a local maximum at $r = 0.25$ mm. Though these extrema are not very pronounced, their presence shows clearly that a Boolean model with convex grains cannot be a realistic model for the sample, since $S_2(r)$ for such a model is always monotonously decreasing. We see that the range of correlation of the volume measure is around 0.3 mm.

Figure 12 shows the probability density functions of the random curvature measure values $C_i(b(x,R))$ for $i = 0,1,2$ and 3 in the style of the local porosity approach for various radii R. For $i = 3$ the values $C_3(b(x,R)) = 0$ and $C_3(b(x,R)) = V(b(x,R))$ are possible, which explains the particular shape of the curve. For $i = 0,1$ and 2 the measures are surface concentrated and zero, if no surface is contained in the measurement sphere. Above $R \approx 13$ ($R \approx 75\,\mu$m) a threshold is reached, for which the observation window never fits into the pore space. The analogue is true for the grain phase above $R \approx 35$ ($R \approx 200\,\mu$m). These thresholds were derived exactly by finding the maximal inscribed sphere size for each phase. For a grain pack with uncorrelated grains one would expect that at this length the correlations vanish, which is in agreement with Figure 11b, considering that the grains are actually not spherical.

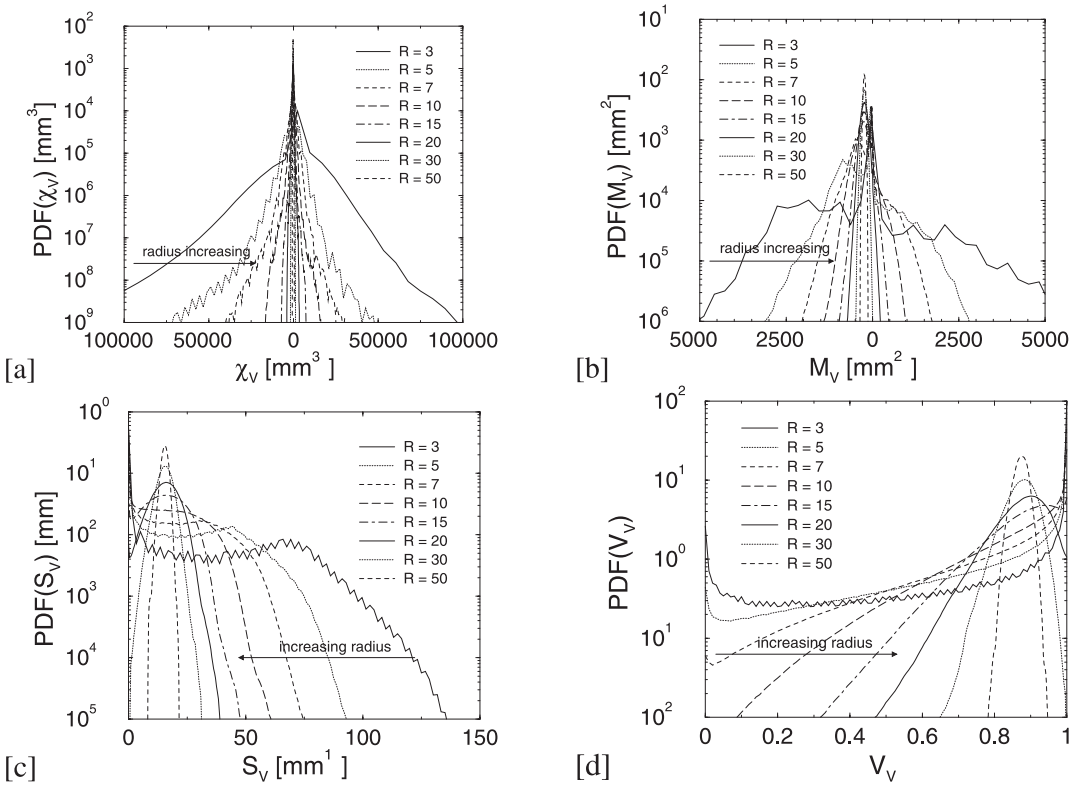

Fig. 12. Probability density functions for the normalized curvature measures $C_i(b(o,R))/V(b(o,R))$ of Fontainebleau sandstone based on different observation window sizes (balls of radius R in voxel units). For small radii the observation window can lie fully in one phase. For S_V, M_V, and χ_V this leads to a sharp peak at 0 for small radii.

Figure 13 shows the variances of the normalized curvature measures $C_i(b(o,R))$ given in Figure 12 for different radii. Clearly with increasing radius R the variance of the curvature intensities decreases. Further, for large radii the measures scale linearly over the inverse of the measurement support volume $V(b(o,R))$. The scaling transition indicates the radius R of the measurement sphere, at which correlations vanish. For χ_V and M_V this is $R \approx 40\,\mu$m and for S_V and V_V it is $R \approx 0.1$ mm.

In the geostatistical approach three spherical windows were used, with radii $R = 5$,10 and 25 voxels. Figure 14 shows the normalized variograms $\gamma_i(r)$ for $i = 0, 1, 2, 3$ and $R = 5$, 10 and 25 voxels (or $R = 28.4$, 56.8 and 142 μm). As expected, the curves become smoother with increasing R. While for $R = 25$ all structure information is smoothed away, for $R = 10$ maxima and minima are still visible. As expected due to equation (16), they are at the same places as those of $S_2(r)$; since covariance function and variogram are connected by equation (24), there is a maximum of $\gamma_3(r)$ where $S_2(r)$ has a minimum and vice versa. Thus it is clear that $\gamma_3(r)$ yields nearly the same structural information as $S_2(r)$ for window radii R not too large. Also $\gamma_3(r)$ says that the range of correlation for the volume measure is about 0.3 mm.

The spatial correlations for the surface measure as shown by γ_2 seem to be nearly the same as for the volume measure. In contrast, the variograms for $C_{X,0}$ and $C_{X,1}$ show a different form. The range of spatial correlation as expressed by the variograms seems to be clearly shorter than that for $C_{X,2}$ and $C_{X,3}$. Thus the similarity of the pore surface system of the sandstone with the plane model is also expressed in the correlation functions. We can conclude that the variability of volume and surface are higher than that of mean curvature and Euler

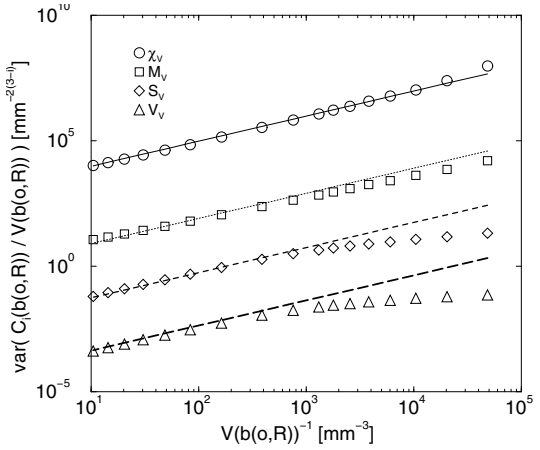

Fig. 13. Scaling of the normalized variances of the curvature measures of Fontainebleau over measuring support volume. The straight lines indicate fits running towards (0, 0) of the coordinate system. For large radii R the variances scale linearly, indicating the measuring window size at which correlations disappear.

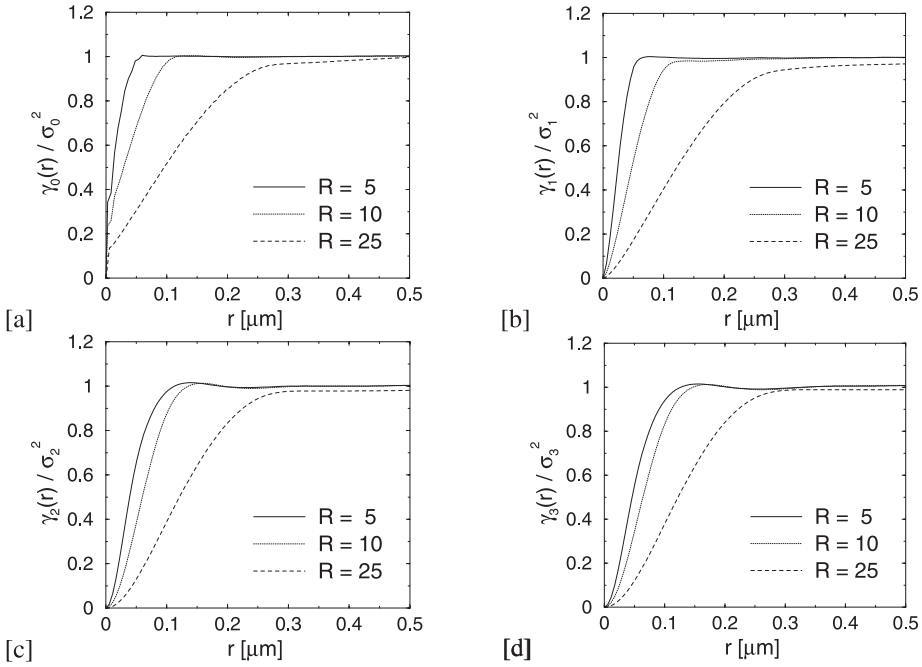

Fig. 14. Variograms $\gamma_i(r)$ of the intrinsic volumes and curvature measures $C_{X,i}(B)$ of Fontainebleau sandstone for $R = 5$, 10 and 25 voxels. [a] Euler characteristic χ_V, [b] integral mean curvature M_V, [c] surface area, S_V, [d] volume V_V.

characteristics. Consequently, when estimating M_V and N_V smaller windows are sufficient, while large windows are required for V_V and S_V.

7 Conclusions

A systematic second-order theory for all four intrinsic volumes of random geometric structures has been presented. Such a theory is necessary since different macroscopic physical properties of materials are correlated to different properties of their microgeometry. These are in close relation to different intrinsic volumes [18,19]. In the present paper it has been demonstrated how one series of these characteristics, the variograms, can be statistically determined using voxel data. The authors believe that PCFs $g_i(r)$ can be estimated for such data (except at small r due to numerical problems). In general variograms give a good description of geometrical variability.

In all examples considered the variograms showed some qualitative differences for the different intrinsic volumes. In particular, variograms corresponding to the Euler characteristic The main difference observed was in the range of correlation; this was clearly shorter for the Euler characteristic. This behaviour is different to the case of a Boolean model, where all intrinsic volumes have the same range of correlation.

C.H.A. acknowledges the Australian Government for their support through the ARC grant scheme (grant DP0558185). We thank Mark A. Knackstedt and Tim J. Senden for providing the industrial foam data sets and the former for a critical reading of the manuscript.

References

1. D. Stoyan, W.S. Kendall, J. Mecke, *Stochastic Geometry and its Applications* (John Wiley & Sons, Chichester, 1995)
2. S. Torquato, *Random Heterogeneous Materials: Microstructure and Macroscopic Properties* (Springer-Verlag, New York, 2002)
3. R. Hilfer, *Statistical Physics and Spatial Statistics - The Art of Analyzing and Modeling Spatial Structures and Pattern Formation*, edited by K.R. Mecke, D. Stoyan, **554** Lect. Notes Phys. (Springer, Berlin, 2000) pp. 203–241
4. K.R. Mecke, *Integralgeometrie in der Statistischen Physik: Perkolation, komplexe Flüssigkeiten und die Struktur des Universums* (Harry Deutsch, Frankfurt, 1994)
5. K. Mecke, Acta Physica Polonica B, **28**, 1747 (1997)
6. K.R. Mecke, Int. J. Mod. Phys. B **12**, 861 (1998)
7. K.R. Mecke, *Statistical Physics and Spatial Statistics - The Art of Analyzing and Modeling Spatial Structures and Pattern Formation*, edited by K.R. Mecke, D. Stoyan, **554** Lect. Notes Phys. (Springer, Berlin, 2000) pp. 111–184
8. M. von Laue, *Münchener Berichte* (1912) p. 303
9. Lord Rayleigh, Proc. Roy. Soc. London Ser. A **84**, 25 (1911)
10. A. Guinier, Ann. Phys. **12**, 161 (1939)
11. P. Debye, H.R. Anderson, H. Brumberger, J. Appl. Phys. **28**, 679 (1957)
12. G. Porod, Kolloid-Zeitschrift **125**, 51; 108 (1952)
13. R. Kirste, G. Porod, Kolloid-Zeitschrift **184**(1), 1 (1962)
14. J.P. Hansen, I.R. McDonald, *Theory of Simple Liquids* (Academic Press, 1976)
15. U. Sonntag, D. Stoyan, H. Hermann, Phys. Stat. Sol. **68**, 281 (1981)
16. P. Smith, S. Torquato, J. Comp. Phys. **76**(1), 176 (1988)
17. K.R. Mecke, J. Stat. Phys. **102**, 1343, (2001)

18. C.H. Arns, M.A. Knackstedt, K.R. Mecke, Phys. Rev. Lett. **91**, 215506 (2003)
19. P.-M. König, R. Roth, K. Mecke, Phys. Rev. Lett. **93**, 1–4 (2004)
20. C.L.Y. Yeong, S. Torquato, Phys. Rev. E **57**, 495 (1998)
21. C.L.Y. Yeong, S. Torquato, Phys. Rev. E **58**, 224 (1998)
22. J.P. Chilès, P. Delfiner, *Geostatistics. Modelling Spatial Uncertainity* (J. Wiley and Sons, New York, 1999)
23. R. Schneider, *Convex Bodies: The Brunn-Minkowski Theory*, *Encyclopedia of Mathematics and its Applications*, Vol. 44 (Cambridge University Press, Cambridge, 1993)
24. D.A. Klain, G.-C. Rota, *Introduction to Geometric Probability* (Cambridge University Press, Cambridge, 1997)
25. A. Tscheschel, D. Stoyan, J. Microsc. **211**, 80 (2003)
26. A. Bezrukov, M. Bargiel, D. Stoyan, Part. Part. Charact. **19**, 111 (2002)
27. S. Torquato, G. Stell, J. Chem. Phys. **79**, 1505 (1983)
28. M. Kerscher, K. Mecke, J. Schmalzing, C. Beisbart, T. Buchert, H. Wagner, Astron. Astrophys. **373**, 1 (2001)
29. U. Brodatzki, K. Mecke, Computer Physics Communications **147**, 218 (2002)
30. Arthur Sakellariou, T.J. Sawkins, T.J. Senden, A. Limaye, Physica A **339**(1-2), 152 (2004)
31. M. Saadatfar, M.A. Knackstedt, C H. Arns, A. Sakellariou, T. Senden, A.P. Sheppard, R.M. Sok, H. Steininger, W. Schrof, Physica A **339**(1-2), 131, (2004)
32. T. Mattfeldt, D. Stoyan, J. Microsc. **200**(2), 158 (2000)
33. D. Marcotte, Computers & Geosciences **22**(10), 1175 (1996)
34. K. Koch, J. Ohser, K. Schladitz, Adv. Appl. Prob. **35**, 603 (2003)
35. W.H. Press, S.A. Teukolsky, W.T. Vetterling, B.P. Flannery, *Numerical Recipes in Fortran 90 - The Art of Parallel Scientific Computing*, Vol. II (Cambridge University Press, Cambridge, 1996)
36. N.A. Seaton, E.D. Glandt, J. Chem. Phys. **85**(9), 5262 (1986)
37. M. Knackstedt, C. Arns, M. Saadatfar, T. Senden, A. Sakellariou, A. Sheppard, R. Sok, W. Schrof, H. Steininger, Adv. Eng. Mat. **7**(4), 238 (2005)
38. A.P. Sheppard, R.M. Sok, H. Averdunk, Physica A **339**(1-2), 145 (2004)
39. P. Spanne, J.F. Thovert, C.J. Jacquin, W.B. Lindquist, K.W. Jones, P.M. Adler, Phys. Rev. Lett. **73**, 2001 (1994)
40. F.M. Auzerais, J. Dunsmuir, B.B. Ferrèol, N. Martys, J. Olson, T.S. Ramakrishnan, D.H. Rothman, L.M. Schwartz, Geophys. Res. Lett. **23**(7), 705 (1996)
41. J.T. Fredrich, Phys. Chem. Earth (A) **24**(7), 551 (1999)
42. J.-F. Thovert, F. Yousefian, P. Spanne, C.G. Jacquin, P.M. Adler, Phys. Rev. E **63**, 61307 (2001)
43. W.B. Lindquist, A. Venkatarangan, J. Dunsmuir, T.F. Wong, J. Geophys. Res. B **105**, 21509 (2000)
44. C.H. Arns, M.A. Knackstedt, W. Val Pinczewski, W.B. Lindquist, Geophys. Res. Lett. **28**(17), 3361 (2001)
45. C.H. Arns, M.A. Knackstedt, K.R. Mecke, *Morphology of Condensed Matter — Physics and Geometry of spatially complex Systems*, edited by K.R. Mecke, D. Stoyan, Lect. Notes Phys. **600** (Springer, Berlin, 2002) pp. 37–74
46. C.H. Arns, M.A. Knackstedt, W.V. Pinczewski, E.G. Garboczi, Geophys. **67**(5), 1396 (2002)
47. C.H. Arns, M.A. Knackstedt, W.V. Pinczewski, N. Martys, J. Petr. Sc. Eng. **45**(1-2), 41 (2004)
48. W. Oh, W. Brent Lindquist, IEEE T. Patt. Anal. Machine Intelligence **21**, 590 (1999)
49. W.B. Lindquist, A. Venkatarangan, Phys. Chem. Earth (A) **25**, 593 (1999)
50. D.J. Bergman, K.-J. Dunn, L.M. Schwartz, P.P. Mitra, Phys. Rev. E **51**, 3393 (1995)